NASA/TM—2008-215421 AIAA–2008–4757

LOX/Methane Main Engine Igniter Tests and Modeling

Kevin J. Breisacher
Glenn Research Center, Cleveland, Ohio

Kumud Ajmani
Arctic Slope Research Corporation, Cleveland, Ohio

November 2008

NASA STI Program . . . in Profile

Since its founding, NASA has been dedicated to the advancement of aeronautics and space science. The NASA Scientific and Technical Information (STI) program plays a key part in helping NASA maintain this important role.

The NASA STI Program operates under the auspices of the Agency Chief Information Officer. It collects, organizes, provides for archiving, and disseminates NASA's STI. The NASA STI program provides access to the NASA Aeronautics and Space Database and its public interface, the NASA Technical Reports Server, thus providing one of the largest collections of aeronautical and space science STI in the world. Results are published in both non-NASA channels and by NASA in the NASA STI Report Series, which includes the following report types:

- TECHNICAL PUBLICATION. Reports of completed research or a major significant phase of research that present the results of NASA programs and include extensive data or theoretical analysis. Includes compilations of significant scientific and technical data and information deemed to be of continuing reference value. NASA counterpart of peer-reviewed formal professional papers but has less stringent limitations on manuscript length and extent of graphic presentations.

- TECHNICAL MEMORANDUM. Scientific and technical findings that are preliminary or of specialized interest, e.g., quick release reports, working papers, and bibliographies that contain minimal annotation. Does not contain extensive analysis.

- CONTRACTOR REPORT. Scientific and technical findings by NASA-sponsored contractors and grantees.

- CONFERENCE PUBLICATION. Collected papers from scientific and technical conferences, symposia, seminars, or other meetings sponsored or cosponsored by NASA.

- SPECIAL PUBLICATION. Scientific, technical, or historical information from NASA programs, projects, and missions, often concerned with subjects having substantial public interest.

- TECHNICAL TRANSLATION. English-language translations of foreign scientific and technical material pertinent to NASA's mission.

Specialized services also include creating custom thesauri, building customized databases, organizing and publishing research results.

For more information about the NASA STI program, see the following:

- Access the NASA STI program home page at *http://www.sti.nasa.gov*

- E-mail your question via the Internet to *help@sti.nasa.gov*

- Fax your question to the NASA STI Help Desk at 301–621–0134

- Telephone the NASA STI Help Desk at 301–621–0390

- Write to:
  NASA Center for AeroSpace Information (CASI)
  7115 Standard Drive
  Hanover, MD 21076–1320

NASA/TM—2008-215421 AIAA–2008–4757

LOX/Methane Main Engine Igniter Tests and Modeling

Kevin J. Breisacher
Glenn Research Center, Cleveland, Ohio

Kumud Ajmani
Arctic Slope Research Corporation, Cleveland, Ohio

Prepared for the
44th Joint Propulsion Conference and Exhibit
sponsored by AIAA, ASME, SAE, and ASEE
Hartford, Connecticut, July 21–23, 2008

Prepared under Contract NNC05BAZZB and NNC08JF17T

National Aeronautics and
Space Administration

Glenn Research Center
Cleveland, Ohio 44135

November 2008

Acknowledgments

The authors wish to thank Lynn Arrington, Rick Gardins, Gerald Hurd, Kim Kearns, Anthony Ogorzaly, Jason Wendell, and Joseph Zoeckler in applying their considerable technical skills in preparing and operating the test facility for the experimental tests described in this paper.

This report contains preliminary findings, subject to revision as analysis proceeds.

Level of Review: This material has been technically reviewed by technical management.

Available from

NASA Center for Aerospace Information
7115 Standard Drive
Hanover, MD 21076–1320

National Technical Information Service
5285 Port Royal Road
Springfield, VA 22161

Available electronically at http://gltrs.grc.nasa.gov

LOX/Methane Main Engine Igniter Tests and Modeling

Kevin Breisacher
National Aeronautics and Space Administration
Glenn Research Center
Cleveland, Ohio 44135

Kumud Ajmani
Arctic Slope Research Corporation
Cleveland, Ohio 44135

Abstract

The LOX/methane propellant combination is being considered for the Lunar Surface Access Module ascent main engine propulsion system. The proposed switch from the hypergolic propellants used in the Apollo lunar ascent engine to LOX/methane propellants requires the development of igniters capable of highly reliable performance in a lunar surface environment. An ignition test program was conducted that used an in-house designed LOX/methane spark torch igniter. The testing occurred in Cell 21 of the Research Combustion Laboratory to utilize its altitude capability to simulate a space vacuum environment. Approximately 750 ignition test were performed to evaluate the effects of methane purity, igniter body temperature, spark energy level and frequency, mixture ratio, flowrate, and igniter geometry on the ability to obtain successful ignitions. Ignitions were obtained down to an igniter body temperature of approximately 260 R with a 10 torr backpressure. The data obtained is also being used to anchor a CFD based igniter model.

Nomenclature

light	ignition obtained
O/F	oxidizer to fuel ratio
P_{cpi}	igniter chamber pressure prior to ignition
P_{Finj}	pressure measured downstream of the fuel valve
P_{Finl}	pressure measured at the inlet of the fuel valve
P_{Oinj}	pressure measured downstream of the oxidizer valve
P_{Oinl}	pressure measured at the inlet of the oxidizer valve
P_{Ftnk}	pressure in the fuel run tank
P_{Otnk}	pressure in the oxidizer run tank
SPS	sparks per second
T_b	igniter body temperature
T_{Finj}	temperature measured downstream of the fuel valve
T_{Finl}	temperature measured at the inlet of the fuel valve
T_{Oinj}	temperature measured downstream of the oxidizer valve
T_{Oinl}	temperature measured at the inlet of the oxidizer valve
W_{CH4}	flowrate of methane
W_{O2}	flowrate of oxygen
head	flow through the injection elements excluding the internal cooling flow
pilot	the reduced flowrates upon the valve first opening
main	the final flowrates during a test

Introduction

The LOX/methane propellant combination is being considered for the Lunar Surface Access Module ascent main engine propulsion system. The LOX/methane propellant combination is being considered for a variety of reasons. This propellant combination would replace toxic propellants that may pose an operational challenge near a lunar base. Use of this propellant combination for lunar ascent would provide operational experience relevant to its use on other planetary bodies where it may be produced from indigenous materials. The proposed switch from the hypergolic propellants used in the Apollo lunar ascent engine to LOX/methane propellants requires the development of igniters capable of highly reliable performance in a lunar surface environment. There has been a flurry of recent activities (ref. 1) to develop such igniters in industry, academia, and at government laboratories. An ignition test program was conducted at the NASA Glenn Research Center (GRC) that used an in-house designed LOX/methane spark torch igniter and the vacuum test facilities in Cell 21 of the Research Combustion Laboratory (RCL) at GRC.

Igniter Hardware

The igniter was a three piece modular design consisting of a head end, a chamber section, and a fuel coolant sleeve as shown in figures 1, 2, and 3. At the top of the igniter head end, are the propellant inlets to which the valve offsets were attached. The valve offsets were small tubes attached to the valves at one end and threaded into the igniter head at the other end. The valve offsets were instrumented with a thermocouple inserted into the flow as well as pressure transducer located on a tube brazed into the offset. The oxygen propellant inlet (on the left in figure 1) feeds a ring manifold with five petals. Four petals of this oxygen manifold each feed a canted impinging injection element that injects oxygen through the top face of the igniter. The methane propellant inlet (on the right in figure 1) feeds a ring manifold running behind the chamber wall at the head end of the igniter. The methane manifold feeds four canted impinging injection elements as well as four tangential inlets (the tear shaped surfaces in figure 1) to swirl the interior coolant flow. The methane injection elements inject through the side of the chamber wall and are located between the oxygen elements on the face. The flow split between the methane injection elements and the swirled internal cooling flow is controlled by the relative flow areas of these passages and is fixed. Additional cooling was provided by a separately controlled methane flow that was directed down between the exterior of the igniter tube and the interior of the coolant sleeve.

A low tension sparkplug was used to ignite the propellants. The sparkplug was mounted in the center of the igniter and for most tests was flush with the top face of the igniter. A variable spark energy (0.007–0.55 J) and sparkrate (to 196 SPS) exciter was used to fire the sparkplug.

Igniter body temperatures were measured by two spring loaded thermocouples mounted in taps on the sides of the igniter. Small tubes were used to mount the valves to the igniter head. These tubes offset the valves from the igniter body to permit the installation of a pressure tap and thermocouple to measure propellant temperatures and pressures downstream of the valve. Propellant flowrates were measured by differential pressure measurements across a calibrated orifice as well as by a turbine flowmeter.

Facility Description

The LOX/LCH4 igniter was tested at the NASA Glenn Research Center (GRC) in RCL-21, which is an altitude test stand used for testing low thrust class rockets. The igniter mounted on the test stand in RCL-21 with the ejector can pulled back is shown in figure 4. The altitude is maintained by an air driven ejector train capable of simulating 95,000 ft (10 torr or 0.2 psia). A laboratory propellant feed system capable of supporting cryogenic propellants was used. This feed system condensed gaseous oxygen and gaseous methane in small propellant tanks using a liquid nitrogen cooling system. The liquid nitrogen lines also traced the propellant lines from the tank to the igniter inlet valves to help ensure the propellants remained in a liquid state up to the igniter manifold. Control relays cycled the liquid nitrogen on and off to each circuit based on the desired tank temperature (90 K for the liquid oxygen, 112 K for the liquid methane). Each bottle held about 2 liters of propellant. The liquid propellants were pressurized by the regulated gaseous propellant feed system with pressures up to 2760 kPa (400 psia). Tests were initiated by a programmable logic controller which triggered a sparkplug controller to time the valves and spark. Figure 5 shows a successful ignition test recorded on video by use of a window and mirror arrangement in the ejector can. For most of the cold body igniter tests the hardware was chilled by flowing ("burping") propellant through the igniter. For a few of the coldest test cases it was necessary to utilize a liquid nitrogen flow loop (fig. 6) to further chill the hardware.

Igniter Modeling

The National Combustor Code (NCC) (ref. 2) was used to perform unsteady simulations of the ignition process in the GRC main engine igniter. The NCC is a state-of-the-art computational tool which is capable of solving the time-dependent, Navier-Stokes equations with chemical reactions. The NCC is being developed primarily at GRC in order to support combustion simulations for a wide range of applications, and has been extensively validated and tested for low-speed chemically reacting flows.

Second-order accurate central-differences are used for the inviscid and viscous flux discretizations, and a Jameson operator (a blend of 2nd and 4th-order dissipation terms) is used to maintain numerical stability. In order to enhance convergence acceleration in pseudo-time, implicit residual smoothing is used to smooth the computed residuals. Dual time-stepping is used to obtain second-order time-accuracy for time-accurate simulations.

Turbulence closure is obtained by a low-Reynolds number two-equation k-e model. A finite-rate chemistry model is used to compute the species source-terms for methane/oxygen chemistry. The chemistry model incorporates 9 species and 7 chemical reaction steps and is detailed in table 1. The model is based on the Sandia National Lab 1D flame methane/air kinetics model (ref. 3) with the reactions involving nitrogen as a species removed. The Peng-Robinson equation of state is used to calculate thermodynamic quantities.

A three-dimensional grid of the igniter flowpath was developed (fig. 7). The flowpath modeled the igniter geometry downstream of the valves and included the drills to the fuel and oxidizer manifolds. The fuel manifold is the annular structure surrounding the top of the igniter. The oxidizer manifold is the annular ring with five petals on the top surface of the igniter. The fuel and oxidizer injection elements, the tangential fuel cooling inlets, the combustion chamber, and exhaust tube are modeled as well.

In a typical simulation propellants are blown down the igniter until methane reaches the end of the exhaust tube. Energy equivalent to the spark used in the tests is then deposited in a region corresponding to the tip of the sparkplug. The dimensions of this region are an approximation of the spark region observed from video of the plug firing. The simulation is then continued until either the flame progresses down the exhaust tube or the flame is observed to go out.

Experimental Test Results

A series of tests were conducted with the GRC igniter design to find the ignition boundaries of LOX/methane ignition in simulated lunar conditions (i.e., vacuum and cold soaked hardware) and provide data to develop CFD based methane igniter models.

The first test series explored the ignition boundaries without the effects of cold soaking the igniter hardware. This test series utilized gaseous propellants and were conducted with 10 torr backpressures. The tests had a long blow down duration (~250 ms) to establish a steady flowfield in the igniter before the sparkplug was fired. This also allowed a steady state condition to be used to model the initial flowfield in the igniter. The tests also had a significant duration (~300 ms) after ignition. A typical propellant valve and sparkplug timing sequence is shown schematically in figure 8. The flowrates for these ignition tests ranged from 0.008 to 0.12 lb/s for both propellants. Typical operating parameters for these tests are provided in table 2. The inlet conditions in tables 2 and 3. ($T_{Oinl,}$ T_{Finl}, P_{Oinl}, P_{Finl}) are measured upstream of the propellant valves. The injection conditions in tables 2 and 3. (T_{Oinj}, T_{Finj}, P_{Oinj}, P_{Finj}) are measured on the valve offsets just down stream of the valves. The valve offsets are small instrumented tubes between the outlet of the propellant valves and the inlets on the igniter head. Typically if ignition occurred, it occurred on the first pulse of the sparkplug. Ignition was confirmed visually (fig. 5), with a thermocouple in the exhaust, and by the rise in igniter chamber pressure. In figure 9, successful ignition tests are indicated by a red 'Y' and a test without a successful ignition test is indicated by a blue 'N'. Not surprisingly, the ignition boundary occurs at fuel rich conditions (fig. 9 and table 2) with ignition failures starting to occur at mixture ratios of 1.57.

More insight can be gained into the ignition boundary observed experimentally by looking at the results of the CFD simulations. Simulations were carried out for two tests (run 1204 and run 1205) that straddle the ignition boundary for the warm igniter tests observed in figure 9. The propellant flowrates for test 1204 were 0.038 lb/s of methane and 0.041 lb/s of oxygen. The propellant flowrates for test 1205 were 0.0199 lb/s of methane and 0.0081 lb/s of oxygen. The overall mixture ratio (including the swirled cooling flow) is 1.08 for test 1204 and 0.4 for test 1205. A head end mixture ratio can be calculated with just the injection element propellant flows near the igniter head end and neglecting the swirled internal methane cooling flow. The flow split between the injection element methane and the swirled cooling methane is determined based on the difference in flow areas. This head end mixture ratio may be more representative of the mixture ratio in the spark region. For test 1204 this head end mixture ratio is 1.8 and for test 1205 it is 0.668. The igniter body temperature for tests 1204 and 1205 was 491 R. As shown in figures 10 and 11, the model correctly captures the ignition in test 1204 and the extinguishment of test 1205. For test 1204 (fig. 10), the flame rapidly spreads throughout the igniter chamber, remains anchored at the face, and exits the igniter tube. As shown in figure 11, the temperature contours show an ignition kernel forms near the spark region and is then pinched off and extinguished as it moves downstream for test 1205 that did not achieve a successful ignition. This would be consistent with the head end (spark region) mixture ratio for test 1205 being above the flammability limit but falling below the flammable mixture ratio as some of the internal cooling methane begins to be mixed in.

Computed mixture ratio profiles at 1.5, 3.0, and 4.5 mm respectively downstream of the igniter face (within the axial extent of the spark region) for tests 1204 and 1205 are shown in figure 12. These profiles are shown after propellant blowdown has been completed but before a spark has been introduced into the simulation. It is clear in figure 12 that the mixture ratios, range of mixture ratios, and the physical extent of oxygen rich areas are all smaller for test 1205 which did not light.

The next test series explored the effect of having cold igniter hardware on the ability to ignite. Although a flight ignition system may employ an igniter body heater, the cold igniter testing was performed to gauge how much heating must be provided and to see how well the igniter would perform in the absence of a heater. Typically, in a sweep of igniter body temperatures the propellant tank pressures were set to produce the desired range of propellant flowrates. The igniter body was then chilled by cold flowing each propellant circuit sequentially through the igniter injection and cooling elements and exhausting into the vacuum can. When the target igniter body temperature was obtained (as measured by two spring loaded thermocouples attached to the igniter) an ignition test was conducted. For some of the coldest igniter body temperatures tested, a coil was used to flow liquid nitrogen around the exterior of the igniter for further chilling. These tests used a more conventional timing sequence with the spark plug being fired within milliseconds of the propellant valves being commanded to open (fig. 13). The spark energy for these tests was typically 250 mJ at 153 sparks per second (SPS). The valve sequence provided a smaller pilot flow for both propellants before the main igniter flow was obtained. A typical oxygen propellant flowrate time history is shown in figure 14. Table 3 provides typical operating conditions for the cold igniter body tests. The mixture ratios provided in table 3 are for both the pilot flow at valve opening and the main flowrates achieved during a run. For both the main and pilot flows, a head end mixture ratio which is based solely on injection element flows (neglecting the internal methane coolant flow) is provided. For test runs 1634 through 1639, a comparison of the inlet conditions in table 3 and the saturation conditions for both methane and oxygen provided in table 4 show that the propellants at the valve inlets were liquid. The injection conditions (downstream of the valves) show that the propellants quickly flash upon seeing the low backpressure (approximately 10 torr) maintained on the igniter. Tests 1634 through 1639, with liquid propellants at the valves, were all successful ignitions. The lowest igniter body temperatures at which ignition could be obtained for the cases with liquid propellants at the valve inlets is higher than those tests with cold gas at the valve inlets ((194 K (349 R) versus 156K (280 R) in table 3.)) By varying tank set pressures (and thus total flowrates, mixture ratios, and propellant quality, figure 15), ignition could be obtained at progressively lower igniter body temperatures.

The results of CFD simulations of tests 1602 and 1603 which straddle the cold igniter body ignition boundary are shown in figures 16 and 17. In these simulations, the appropriate igniter wall temperature was imposed as a boundary condition. The temperature contour plots for test 1603 (fig. 17) show an ignition kernel forming and getting pinched off. This is similar to the results for test 1205 (fig. 11) which did not ignite with a warm igniter body. The results for the successful cold body ignition case, tests 1602, show that the ignition kernel does not propagate to the igniter walls in the manner that a successful warm body ignition test does (fig. 10). Axial mixture ratio profiles for tests 1603 and 1604 (fig. 18) show a similar reduction in mixture ratio and oxidizer rich regions near the spark region as those computed for the warm igniter body boundary (fig. 12). The reduction in mixture ratio for the test in which no ignition was obtained for the cold body does not appear to be quite as severe as the case for which no ignition was achieved with a warm igniter body (test 1205, figure 12). A look at the axial temperature profiles for the cold igniter body test cases in the spark region (fig. 19), shows that the successful ignition case (test 1603) appears to be insulated from the cold walls and cooling flows by a region of relatively warmer gas.

Test series with the same operating set conditions were performed to gauge the effect of a particular operating parameter (i.e., spark plug power, etc.) on the cold igniter wall ignition characteristics. The results for each parameter investigated are presented below.

Sparkplug Power

The power delivered to the sparkplug was varied by fixing the sparkrate at 153 SPS and varying the energy per spark. This resulted in power settings of 6.12 W at 40 mJ/spark, 10.71 W at 70 mJ/spark, 22.95 W at 150 mJ/spark, and 39.78 W at 260 mJ/spark respectively. Ignition tests at various igniter body temperatures at fixed tank set pressures were conducted. There does not appear to be a significant change in the ability to ignite except possibly below 10 W. Below a power of 10 W, the ability to ignite at the coldest igniter body temperatures may begin to be affected (fig. 20).

Energy Per Spark

The power delivered to the spark plug was held constant at approximately 33 W and the energy per spark and sparkrate were adjusted. There does not appear to be a significant change in the ability to ignite until the lower bound of spark energy tested, 17 mJ, is approached (fig. 21).

Sparkplug Recess

For the majority of the tests with this igniter, the face of the sparkplug was flush with the top surface of the igniter chamber (no recess) as shown in figure 1. A series of tests were run with the sparkplug shimmed back so that the tip of sparkplug was recessed approximately 0.0038 m (0.15 in.) behind the top surface of the igniter chamber. Ignition tests at various igniter body temperatures at fixed tank set pressures were conducted. These tests were at similar operating points to tests conducted when the sparkplug was not recessed. As shown in figure 22, recessing the sparkplug significantly degraded the igniter body temperature threshold at which successful ignitions could be obtained. It is theorized that the walls of the recessed region provided additional surface area to quench the spark kernel.

Fuel Purity

The sensitivity of ignition to the purity of the methane at these operating conditions was explored. Most of the tests documented in this report used methane with less than 100 ppm concentrations of ethane, propane, and nitrogen. Ignition tests were conducted with methane with greater impurities consisting of concentrations of 4990 ppm ethane, 3060 ppm propane, and 3010 ppm nitrogen these tests duplicated operating conditions tested for the pure methane in which igniter body temperature was ramped downward at three different tank set pressures. There was no significant change in the ability to ignite (fig. 23).

Nozzle

To simulate the rise in chamber pressure as propellants flow into the main engine during a start-up sequence, a small chamber with a 0.15 in diameter nozzle was placed on the back of the igniter hardware.

The small copper chamber and nozzle mounted to the igniter can be seen in figure 6. Ignition tests at three tank set pressures were conducted at altitude. The ignition boundary for these tests is shown in figure 24. A comparison of figure 24 and 15 shows an increase in the cold igniter boundary temperatures particularly at the lower tank set pressures. This may be due to increased heat loss to the walls as effective igniter chamber pressure is increased.

Summary

The fuel rich boundary for an impinging element, LOX/methane spark torch igniter at altitude was determined experimentally. The fuel rich ignition boundary was determined with a cold igniter body at altitude. The effects of energy per spark, sparkplug power, spark plug recess, and methane purity on this ignition boundary were determined. Three-dimensional, transient CFD simulations of the igniter were performed and compared to test results.

References

1. Studak, J., Schnieder, S., and Grimm, T., "LOX/CH4 Ignition Results With Aerojet RCS LOX/Ethanol Igniter," JANNAF Propulsion Meeting, May 2007.
2. Liu, Nan-Suey, "Overview of the NCC," NASA/CP—2001-211141, proceeding of the Tenth Thermal and Fluids Analysis Workshop, July 2001.
3. Schneider, Ch., Dreizler, A., and Janicka, J., "Flowfield Measurements of Stable and Locally Extinguishing Hydrocarbon Fueled Jet Flames," Combust. Flame 135:185–190 (2003).

TABLE 1.—O_2/CH_4 CHEMICAL KINETICS MODEL

No.	Reaction	A	n	E
1	$CH_4 + 2O_2 <=> CO_2 + 2H_2O$	6.70E+11	0.0	48400.0
2	$H_2 + O_2 <=> H_2O + O$	5.00E+12	1.0	4.80E+4
3	$H_2 + O <=> H + OH$	2.50E+14	0.00	6.00E+3
4	$H + O_2 <=> O + OH$	4.00E+14	0.00	1.80E+4
5	$CO + OH <=> CO_2 + H$	1.51E+07	1.28	–7.58E+2
6	$O_2 + H_2O <=> 2O + H_2O$	5.00E+18	0.00	1.12E+5
7	$CO + H_2O <=> CO_2 + H_2$	5.50E+04	1.28	–1.00E+3

TABLE 2(a).—STEADY FLOW IGNITION OPERATING CONDITIONS
[Metric]

RUN no.	Spark energy, (mJ)	W_{CH4}, (kg/s)	W_{O2}, (kg/s)	O/F main	Pc_{pi}, (MPa)	T_{Oinj}, (K)	T_{Oinl}, (K)	P_{Oinj}, (MPa)	P_{Oinl}, (MPa)	T_{Finj}, (K)	T_{Finl}, (K)	P_{Fnj}, (MPa)	P_{Finl}, (MPa)	P_{Otnk}, (MPa)	P_{Ftnk}, (MPa)	light	T_b, (K)
1144	400	0.0236	0.0367	1.52	0.194	260	154	0.360	0.500	266	176	0.534	0.737	0.759	0.859	Y	283
1145	400	0.0145	0.0218	1.52	0.258	236	112	0.440	0.656	236	144	0.614	0.838	0.745	0.895	N	282
1146	400	0.0199	0.0318	1.57	0.233	254	133	0.322	0.415	254	159	0.599	0.808	0.691	0.867	N	280
1147	400	0.0213	0.0345	1.60	0.219	257	149	0.445	0.627	257	191	0.566	0.783	0.783	0.864	Y	278
1148	400	0.0240	0.0367	1.65	0.219	258	152	0.491	0.695	258	194	0.551	0.763	0.859	0.859	Y	278
1149	400	0.0530	0.0395	1.65	0.199	261	164	0.407	0.565	261	203	0.521	0.728	1.056	0.855	Y	278
1150	400	0.0195	0.0404	2.07	0.220	261	158	0.392	0.538	261	199	0.578	0.789	0.989	0.872	Y	279
1151	400	0.0177	0.0399	2.29	0.240	258	164	0.542	0.775	258	202	0.600	0.801	1.041	0.871	Y	281
1152	400	0.0209	0.0458	2.18	0.251	257	167	0.647	0.925	262	202	0.552	0.744	1.158	0.873	Y	281
1153	400	0.0041	0.0413	10.10	0.236	259	142	0.537	0.750	263	212	0.537	0.728	1.078	0.841	Y	282
1154	400	0.0218	0.0408	1.87	0.233	259	151	0.440	0.627	263	204	0.548	0.742	1.014	0.866	Y	283
1155	400	0.0041	0.0395	9.30	0.221	257	123	0.399	0.562	262	208	0.537	0.745	0.874	0.943	Y	284
1156	400	0.0222	0.0358	1.60	0.236	257	181	0.486	0.677	261	204	0.560	0.764	0.844	0.870	Y	284
1157	400	0.0041	0.0367	9.23	0.207	256	184	0.400	0.556	266	221	0.521	0.734	0.797	0.878	Y	282
1158	400	0.0045	0.0054	1.23	0.199	252	181	0.411	0.587	264	218	0.523	0.749	0.715	0.860	N	283
1159	400	0.0041	0.0059	1.49	0.213	253	180	0.444	0.647	260	209	0.546	0.762	0.781	0.870	N	282
1160	400	0.0218	0.0336	1.56	0.214	253	115	0.306	0.412	258	204	0.552	0.764	0.809	0.862	Y	506
1161	550	0.0041	0.0358	9.23	0.211	249	178	0.447	0.616	259	212	0.513	0.721	0.822	0.862	Y	281
1162	550	0.0045	0.0304	6.94	0.189	251	159	0.267	0.351	258	208	0.513	0.717	0.688	0.849	Y	282
1163	550	0.0041	0.0277	6.60	0.196	249	180	0.394	0.530	258	212	0.531	0.744	0.666	0.862	Y	282
1164	550	0.0045	0.0345	0.79	0.195	451	189	0.339	0.313	260	213	0.546	0.774	0.609	0.906	N	282
1165	550	0.0041	0.0322	7.83	0.192	251	178	0.339	0.471	261	215	0.519	0.731	0.621	0.863	Y	281
1166	550	0.0041	0.0231	5.49	0.186	250	187	0.234	0.297	261	215	0.529	0.752	0.635	0.873	Y	281
1167	550	0.0041	0.0313	7.52	0.200	247	168	0.324	0.448	262	219	0.538	0.765	0.606	0.897	Y	281
1168	550	0.0041	0.0227	5.60	0.188	247	186	0.234	0.293	262	220	0.529	0.747	0.574	0.868	Y	281
1169	550	0.0041	0.0367	9.13	0.200	246	183	0.317	0.434	262	220	0.519	0.738	0.648	0.882	Y	280
1170	550	0.0041	0.0299	7.22	0.206	243	167	0.471	0.650	261	219	0.539	0.743	0.792	0.860	Y	281
1171	550	0.0041	0.0340	8.38	0.192	247	147	0.324	0.440	262	221	0.532	0.753	0.887	0.883	Y	281
1172	220	0.0041	0.0404	9.62	0.202	246	165	0.438	0.636	262	219	0.540	0.744	0.906	0.869	Y	282
1173	220	0.0045	0.0372	8.34	0.204	246	164	0.478	0.666	262	216	0.535	0.733	0.843	0.875	Y	282
1174	220	0.0045	0.0349	8.18	0.204	246	163	0.450	0.638	261	217	0.529	0.743	0.798	0.874	Y	283

TABLE 2(b).—STEADY FLOW IGNITION OPERATING CONDITIONS
[English]

RUN no.	Spark energy, (mJ)	W_{CH4}, (lb/s)	W_{O2}, (lb/s)	O/F, main	Pc_{pi}, (psia)	T_{Oinj}, (R)	T_{Oinl}, (R)	P_{Oinj}, (psia)	P_{Oinl}, (psia)	T_{Finj}, (R)	T_{Finl}, (R)	P_{Fnj}, (psia)	P_{Finl}, (psia)	P_{Otnk}, (psia)	P_{Ftnk}, (psia)	light	T_b, (R)
1144	400	0.052	0.081	1.52	28.30	468	278	52.40	72.70	479	316	77.70	107.20	110.40	125.10	Y	510
1145	400	0.032	0.048	1.52	37.60	425	201	64.10	95.50	425	259	89.40	121.90	108.40	130.30	N	508
1146	400	0.044	0.070	1.57	34.00	457	240	47.00	60.50	457	286	87.20	117.60	100.60	126.20	N	504
1147	400	0.047	0.076	1.60	32.00	463	268	64.70	91.30	463	344	82.40	113.90	113.90	125.70	Y	501
1148	400	0.049	0.081	1.65	32.00	464	273	71.50	101.20	464	350	80.30	111.00	125.00	125.00	Y	501
1149	400	0.053	0.087	1.65	29.00	469	296	59.20	82.20	469	366	75.80	105.90	153.70	124.40	Y	501
1150	400	0.043	0.089	2.07	32.00	469	285	57.10	78.30	469	359	84.10	114.90	144.00	126.90	Y	503
1151	400	0.039	0.088	2.29	35.00	464	296	78.90	112.80	464	363	87.30	116.60	151.50	126.70	Y	505
1152	400	0.046	0.101	2.18	36.50	463	301	94.10	134.70	471	364	80.30	108.30	168.60	127.00	Y	505
1153	400	0.009	0.091	10.10	34.40	466	255	78.10	109.20	473	382	78.10	106.00	156.90	122.40	Y	508
1154	400	0.048	0.090	1.87	33.90	466	272	64.10	91.30	473	367	79.80	108.00	147.60	126.10	Y	510
1155	400	0.009	0.087	9.30	32.10	462	221	58.10	81.80	472	375	78.10	108.50	127.20	137.30	Y	511
1156	400	0.049	0.079	1.60	34.30	462	325	70.80	98.60	469	368	81.60	111.20	122.80	126.70	Y	512
1157	400	0.009	0.081	9.23	30.10	460	331	58.20	80.90	479	397	75.80	106.90	116.10	127.80	Y	508
1158	400	0.010	0.012	1.23	28.90	454	326	59.80	85.50	476	393	76.10	109.00	104.00	125.20	N	509
1159	400	0.009	0.013	1.49	31.00	455	324	64.60	94.20	468	376	79.50	110.90	113.70	126.60	N	508
1160	400	0.048	0.074	1.56	31.10	456	207	44.50	59.90	464	368	80.30	111.20	117.80	125.50	Y	506
1161	550	0.009	0.079	9.23	30.70	448	321	65.10	89.70	467	382	74.60	104.90	119.60	125.40	Y	507
1162	550	0.010	0.067	6.94	27.50	451	287	38.80	51.10	465	375	74.70	104.40	100.20	123.60	Y	508
1163	550	0.009	0.061	6.60	28.50	448	324	57.30	77.20	465	381	77.30	108.30	96.90	125.50	Y	508
1164	550	0.010	0.076	0.79	28.40	451	341	36.20	45.60	468	384	79.40	112.70	88.70	131.90	N	508
1165	550	0.009	0.071	7.83	28.00	448	321	49.30	68.60	469	387	75.60	106.40	90.40	125.60	Y	506
1166	550	0.009	0.051	5.49	27.50	450	337	34.00	43.20	469	387	77.00	109.40	92.40	127.00	Y	506
1167	550	0.009	0.069	7.52	29.10	445	303	47.20	65.20	471	394	78.30	111.30	88.20	130.60	Y	506
1168	550	0.009	0.050	5.60	27.30	445	335	34.00	42.60	472	396	77.00	108.70	83.60	126.30	Y	505
1169	550	0.009	0.081	9.13	29.20	443	330	46.10	63.20	471	396	75.60	107.40	94.30	128.40	Y	504
1170	550	0.009	0.066	7.22	30.00	437	301	68.60	94.60	470	394	78.40	108.10	115.30	125.20	Y	505
1171	550	0.009	0.075	8.38	27.90	445	264	47.20	64.10	471	397	77.40	109.60	129.10	128.50	Y	506
1172	220	0.009	0.089	9.62	29.40	443	297	63.80	92.60	471	394	78.60	108.30	131.90	126.50	Y	507
1173	220	0.010	0.082	8.34	29.70	442	295	69.50	96.90	471	388	77.80	106.70	122.70	127.40	Y	508
1174	220	0.010	0.077	8.18	29.70	442	293	65.50	92.90	469	391	77.00	108.10	116.20	127.20	Y	509

TABLE 3(a).—TYPICAL COLD IGNITER BODY IGNITION TEST PARAMETERS
[Metric]

RUN no.	Spark energy, (mJ)	W_{CH4}, (kg/s) pilot	W_{O2}, (kg/s) pilot	O/F pilot	O/F pilot head	W_{CH4}, (kg/s) main	W_{O2}, (kg/s) main	O/F main	O/F main head	T_{Oinj}, (K)	T_{Oinlt}, (K)	T_{Finj}, (K)	T_{Finl}, (K)	P_{Otnk}, (MPa)	P_{ftnk}, MPa)	light	T_b (K)
1631	260	0.0018	0.0035	2.000	3.34	0.0136	0.0259	1.90	3.17	216	154	208	142	0.914	0.776	Y	229
1632	260	0.0026	0.0025	0.966	1.61	0.0141	0.0249	1.75	2.92	216	150	208	143	0.914	0.770	Y	229
1633	260	0.0026	0.0020	0.740	1.24	0.0141	0.0249	1.78	2.97	210	123	191	143	0.914	0.776	Y	223
1634	260	0.0031	0.0020	0.630	1.06	0.0136	0.0236	1.74	2.91	196	117	183	143	0.921	0.776	Y	217
1635	260	0.0034	0.0020	0.580	0.97	0.0113	0.0195	1.72	2.87	191	117	177	142	0.941	0.770	Y	211
1636	260	0.0019	0.0032	1.750	2.92	0.0113	0.0163	1.44	2.40	185	117	175	142	0.921	0.742	Y	205
1637	260	0.0023	0.0026	1.110	1.85	0.0154	0.0268	1.73	2.89	157	116	174	142	0.900	0.735	Y	199
1638	260	0.0022	0.0037	1.710	2.86	0.0209	0.0290	1.39	2.32	138	117	174	142	0.948	0.742	Y	194
1639	260	0.0022	0.0037	1.710	2.86	0.0218	0.0299	1.36	2.27	138	117	174	142	0.941	0.742	Y	194
1640	260	0.0020	0.0045	2.190	3.66	0.0200	0.0349	1.76	2.94	163	117	180	144	0.934	0.776	N	196
1641	260	0.0023	0.0031	1.330	2.22	0.0177	0.0209	1.19	1.99	210	162	195	166	0.632	0.557	Y	233
1642	260	0.0025	0.0033	1.320	2.20	0.0199	0.0181	1.09	1.82	199	157	183	162	0.632	0.557	Y	223
1643	260	0.0028	0.0036	1.270	2.12	0.0177	0.0245	1.38	2.30	196	157	182	161	0.646	0.598	Y	216
1644	260	0.0032	0.0039	1.240	2.07	0.0168	0.0263	1.57	2.62	192	156	183	162	0.642	0.666	Y	210
1645	260	0.0069	0.0034	0.490	0.82	0.0091	0.0244	2.70	4.51	193	152	178	136	0.642	0.550	Y	205
1646	260	0.0022	0.0036	1.630	2.72	0.0176	0.0259	1.46	2.44	188	154	178	152	0.638	0.543	Y	201
1647	260	0.0023	0.0034	1.490	2.48	0.0172	0.0167	0.97	1.62	156	127	178	156	0.638	0.550	Y	195
1648	260	0.0024	0.0034	1.390	2.32	0.0195	0.0277	1.42	2.37	153	128	174	160	0.646	0.570	Y	190
1649	260	0.0026	0.0043	1.670	2.79	0.0086	0.0249	2.94	4.91	143	126	177	169	0.646	0.563	Y	184
1650	260	0.0028	0.0038	1.360	2.27	0.0195	0.0313	1.60	2.67	151	126	164	164	0.638	0.556	Y	179
1651	260	0.0027	0.0035	1.280	2.14	0.0150	0.0318	2.12	3.54	148	137	164	164	0.646	0.542	N	173
1652	260	0.0025	0.0036	1.410	2.35	0.0154	0.0267	1.73	2.89	158	135	160	157	0.642	0.550	Y	168
1653	260	0.0024	0.0045	1.920	3.21	0.0186	0.0358	1.93	3.22	135	121	161	149	0.646	0.557	N	162
1654	260	0.0029	0.0036	1.210	2.02	0.0154	0.0295	1.91	3.19	182	164	163	157	0.638	0.570	Y	178
1655	260	0.0033	0.0039	1.170	1.95	0.0172	0.0286	1.65	2.76	157	153	167	156	0.642	0.694	Y	173
1656	260	0.0013	0.0040	3.140	5.24	0.0141	0.0313	2.24	3.74	147	139	163	137	0.638	0.549	N	168
1657	260	0.0020	0.0039	2.000	3.34	0.0104	0.0245	2.35	3.92	135	131	173	165	0.522	0.467	Y	178
1658	260	0.0022	0.0035	1.600	2.67	0.0122	0.0304	2.48	4.14	143	134	164	159	0.522	0.502	Y	173
1659	260	0.0015	0.0026	1.710	2.86	0.0163	0.0231	1.41	2.35	144	132	162	137	0.494	0.550	Y	168
1660	260	0.0050	0.0034	0.690	1.15	0.0118	0.0277	2.34	3.91	144	132	154	132	0.522	0.433	Y	162
1661	260	0.0017	0.0034	2.050	3.42	0.0159	0.0286	1.80	3.01	137	131	151	141	0.501	0.447	Y	156
1662	260	0.0021	0.0034	1.630	2.72	0.0159	0.0336	2.11	3.52	138	133	151	143	0.501	0.447	N	151

TABLE 3(b).—TYPICAL COLD IGNITER BODY IGNITION TEST PARAMETERS
[English]

RUN no.	Spark energy, (mJ)	W_{CH4}, (lb/s) pilot	W_{O2}, (lb/s) pilot	O/F pilot	O/F pilot head	W_{CH4}, (lb/s) main	W_{O2}, (lb/s) main	O/F main	O/F main head	T_{Oinj}, (R)	T_{Oinlt}, (R)	T_{Finj}, (R)	T_{Finl}, (R)	P_{Otnk}, (psia)	P_{ftnk}, (psia)	light	T_b, (R)
1631	260	0.0039	0.0078	2.000	3.34	0.030	0.057	1.90	3.17	389	277	375	256	133	113	Y	412
1632	260	0.0058	0.0056	0.966	1.61	0.031	0.055	1.75	2.92	389	270	375	257	133	112	Y	412
1633	260	0.0058	0.0043	0.740	1.24	0.031	0.055	1.78	2.97	378	221	343	257	133	113	Y	401
1634	260	0.0068	0.0043	0.630	1.06	0.030	0.052	1.74	2.91	353	210	329	257	134	113	Y	391
1635	260	0.0074	0.0043	0.580	0.97	0.025	0.043	1.72	2.87	343	211	319	256	137	112	Y	379
1636	260	0.0041	0.0070	1.750	2.92	0.025	0.036	1.44	2.40	333	210	315	256	134	108	Y	369
1637	260	0.0051	0.0057	1.110	1.85	0.034	0.059	1.73	2.89	283	209	313	256	131	107	Y	359
1638	260	0.0048	0.0081	1.710	2.86	0.046	0.064	1.39	2.32	249	210	313	256	138	108	Y	349
1639	260	0.0048	0.0081	1.710	2.86	0.048	0.066	1.36	2.27	249	210	313	256	137	108	Y	349
1640	260	0.0045	0.0099	2.190	3.66	0.044	0.077	1.76	2.94	293	210	324	260	136	113	N	352
1641	260	0.0051	0.0068	1.330	2.22	0.039	0.046	1.19	1.99	378	291	351	298	92	81	Y	419
1642	260	0.0055	0.0073	1.320	2.20	0.044	0.040	1.09	1.82	358	283	330	292	92	81	Y	401
1643	260	0.0062	0.0079	1.270	2.12	0.039	0.054	1.38	2.30	353	283	328	289	94	87	Y	389
1644	260	0.0070	0.0087	1.240	2.07	0.037	0.058	1.57	2.62	345	280	329	292	95	97	Y	379
1645	260	0.0152	0.0075	0.490	0.82	0.020	0.054	2.70	4.51	347	273	321	244	95	80	Y	369
1646	260	0.0049	0.0080	1.630	2.72	0.039	0.057	1.46	2.44	338	277	320	274	93	79	Y	362
1647	260	0.0051	0.0076	1.490	2.48	0.038	0.037	0.97	1.62	281	228	321	281	93	80	Y	351
1648	260	0.0054	0.0075	1.390	2.32	0.043	0.061	1.42	2.37	275	231	314	288	94	83	Y	342
1649	260	0.0057	0.0095	1.670	2.79	0.019	0.055	2.94	4.91	258	227	318	304	94	82	Y	331
1650	260	0.0061	0.0083	1.360	2.27	0.043	0.069	1.60	2.67	272	226	296	296	93	81	Y	322
1651	260	0.0061	0.0078	1.280	2.14	0.033	0.070	2.12	3.54	267	246	295	295	94	79	N	312
1652	260	0.0056	0.0079	1.410	2.35	0.034	0.059	1.73	2.89	285	243	288	283	95	80	Y	303
1653	260	0.0052	0.0100	1.920	3.21	0.041	0.079	1.93	3.22	243	218	290	268	94	81	N	292
1654	260	0.0065	0.0079	1.210	2.02	0.034	0.065	1.91	3.19	328	295	293	282	93	83	Y	321
1655	260	0.0073	0.0086	1.170	1.95	0.038	0.063	1.65	2.76	283	275	300	281	95	101	Y	312
1656	260	0.0028	0.0088	3.140	5.24	0.031	0.069	2.24	3.74	265	251	294	246	93	80	N	303
1657	260	0.0043	0.0086	2.000	3.34	0.023	0.054	2.35	3.92	243	235	311	297	76	68	Y	321
1658	260	0.0048	0.0078	1.600	2.67	0.027	0.067	2.48	4.14	257	241	295	287	76	73	Y	311
1659	260	0.0034	0.0058	1.710	2.86	0.036	0.051	1.41	2.35	259	238	292	246	72	80	Y	303
1660	260	0.0110	0.0076	0.690	1.15	0.026	0.061	2.34	3.91	259	238	277	238	76	63	Y	292
1661	260	0.0037	0.0076	2.050	3.42	0.035	0.063	1.80	3.01	246	235	272	254	73	65	Y	280
1662	260	0.0046	0.0075	1.630	2.72	0.035	0.074	2.11	3.52	248	240	271	257	73	65	N	272

TABLE 4(a).—SATURATION PROPERTIES OF OXYGEN AND METHANE AT IGNITER TEST CONDITIONS
[Metric]

Oxygen		Methane	
Pressure, (MPa)	T (saturation) °K	Pressure, (MPa)	T(saturation) °K
0.52	109.3	0.45	133.4
0.62	111.9	0.58	138.3
0.93	118.4	0.76	143.3

TABLE 4(b).—SATURATION PROPERTIES OF OXYGEN AND METHANE AT IGNITER TEST CONDITIONS
[English]

Oxygen		Methane	
Pressure, (psia)	T (saturation) R	Pressure, (psia)	T(saturation) R
75	196.7	65	240.1
90	201.5	85	248.9
135	213.1	110	258.0

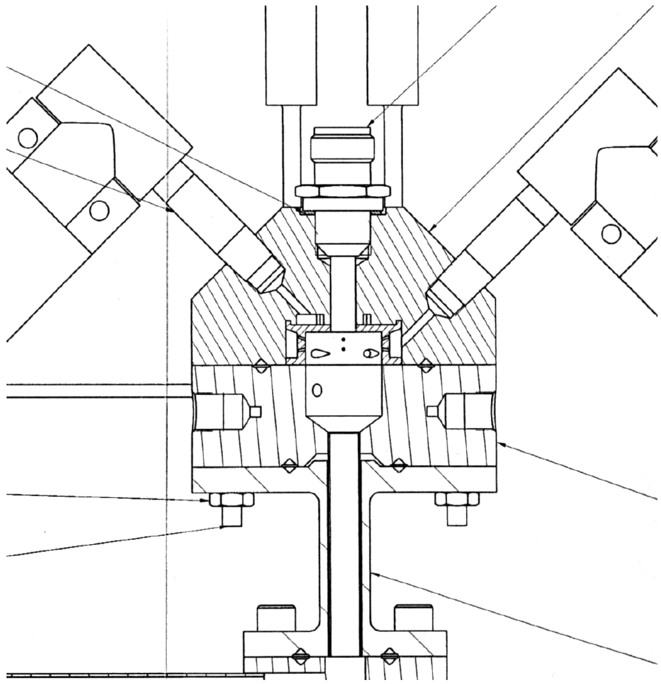

Figure 1.—Cross section of igniter assembly.

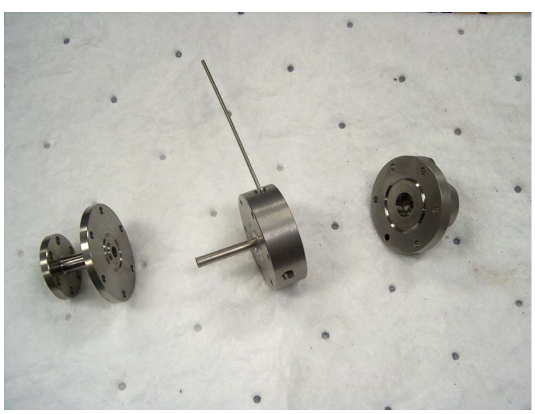

Figure 2.—From right, igniter head end, chamber with center flame tube and pressure port attached, and coolant sleeve.

Figure 3.—Assembled igniter stack.

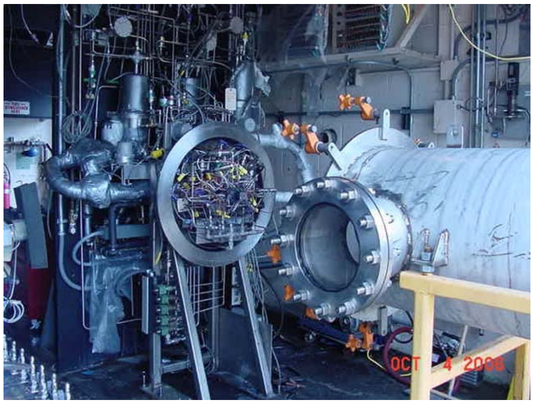

Figure 4.—Igniter mounted on the test Stand in RCL Cell 21 with ejector can pulled back.

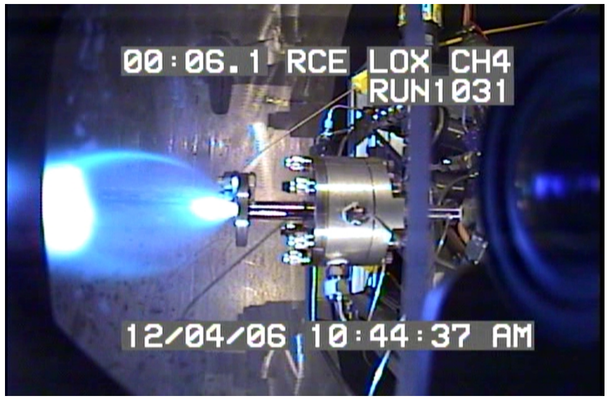

Figure 5.—Successful igniter test in ejector can.

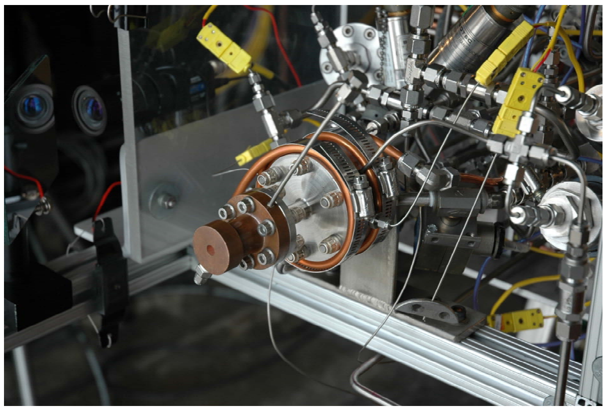

Figure 6.—Igniter with copper nitrogen cooling loop installed.

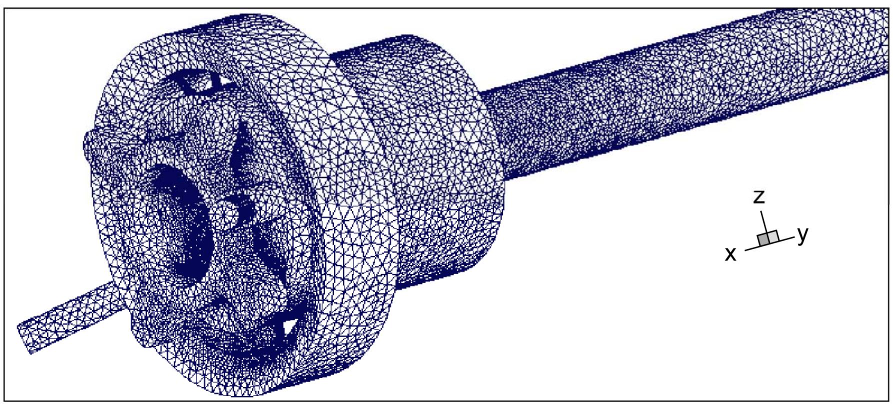

Figure 7.—3D computational mesh of igniter geometry.

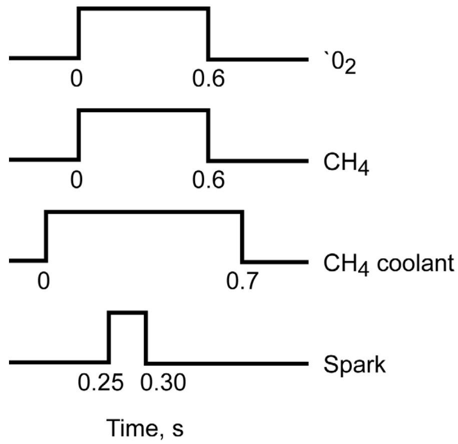

Figure 8.—Timing sequence for long, “steady state” tests.

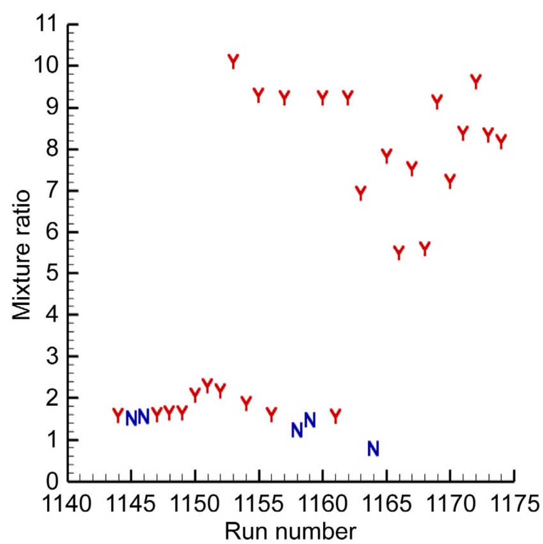

Figure 9.—Ignition boundaries for long duration runs with gaseous propellants and a warm igniter body.

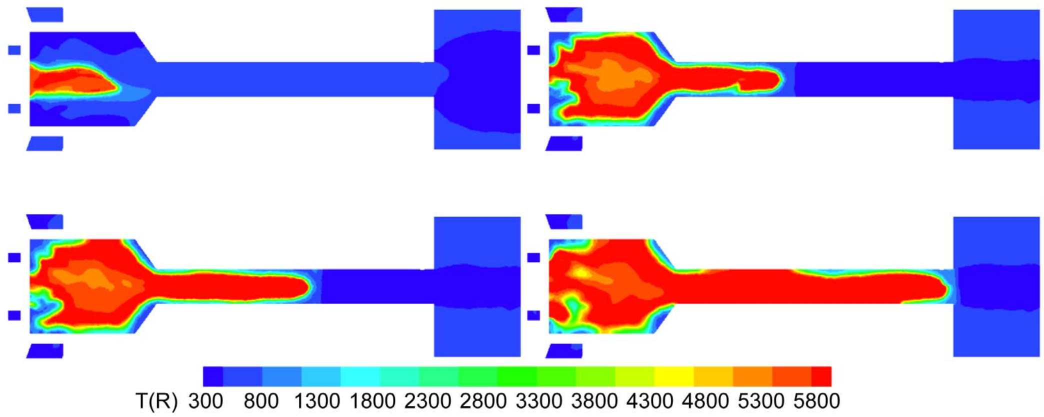

Figure 10.—Transient simulation of test 1204 a successful ignition test (warm igniter body).

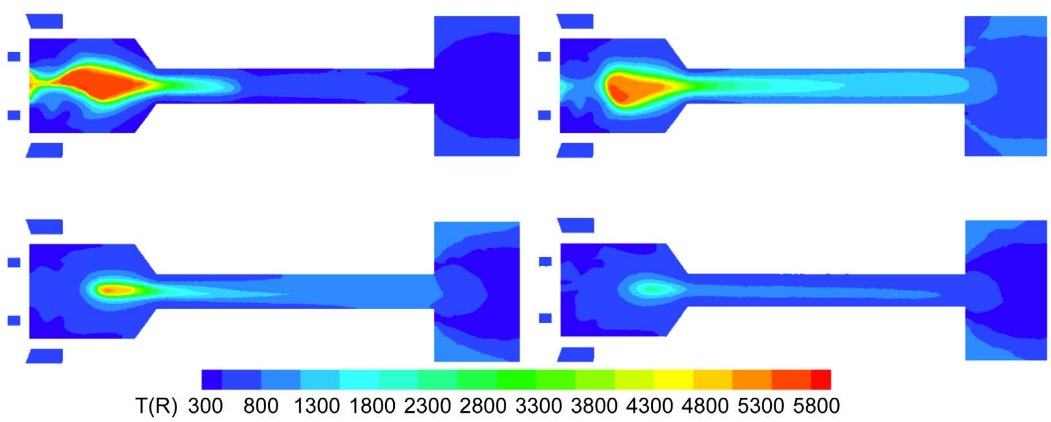

Figure 11.—Transient simulation of test 1205 (warm igniter body) no ignition.

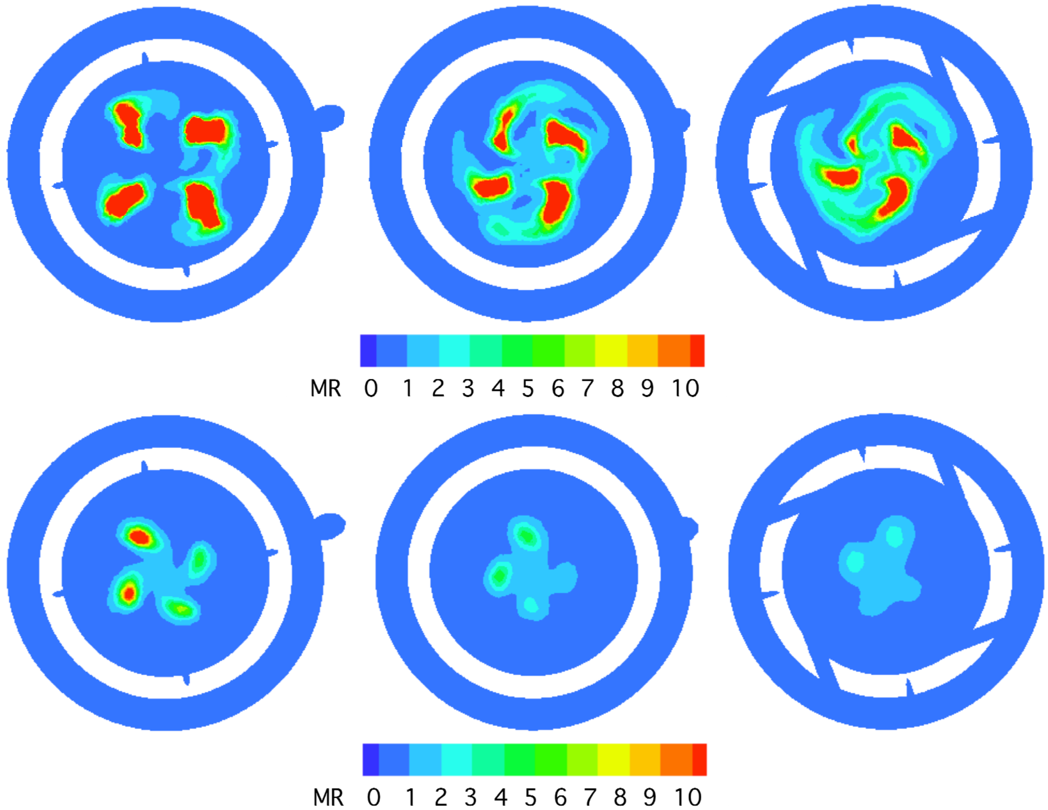

Figure 12.—Comparison of mixture ratio profiles downstream of igniter face in spark region. Successful ignition test 1204 (shown on top) and test 1205 without ignition (shown on the bottom).

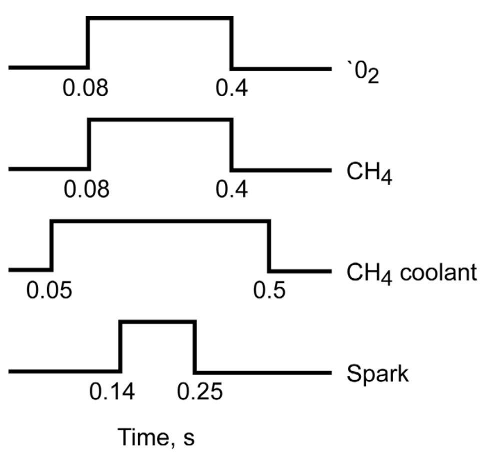

Figure 13.—Igniter timing for short, “normal” ignition test.

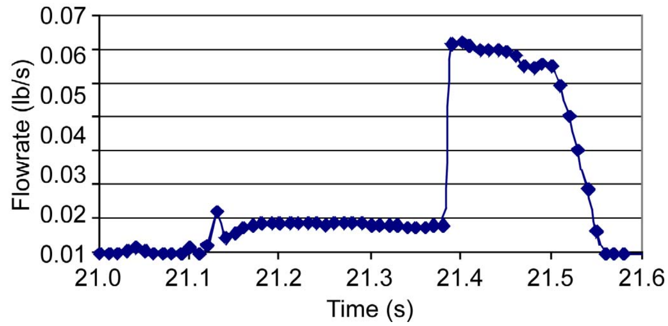

Figure 14.—Typical oxidizer propellant time history.

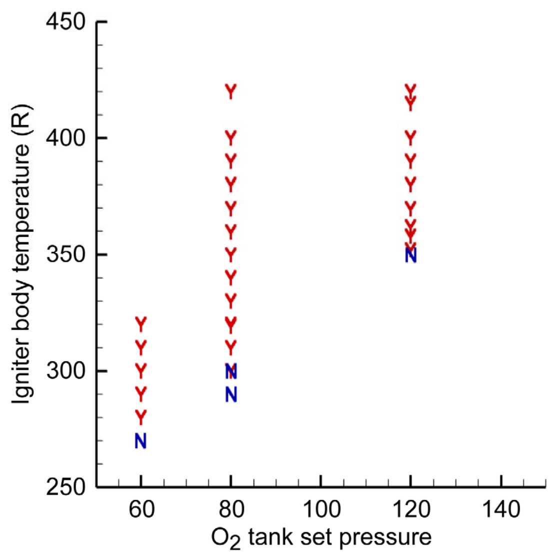

Figure 15.—Cold igniter body ignition boundaries.

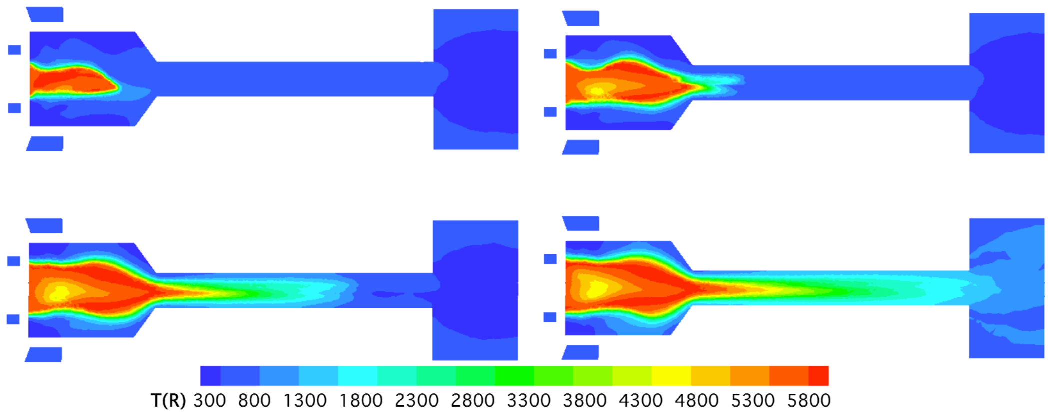

Figure 16.—Transient simulation of test 1602 a successful ignition (cold igniter body).

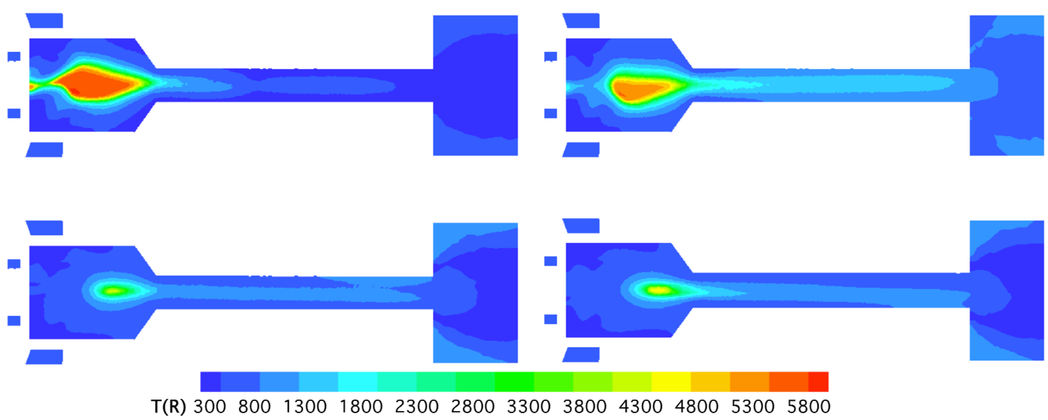

Figure 17.—Transient simulation of test 1603 (cold igniter body) no ignition.

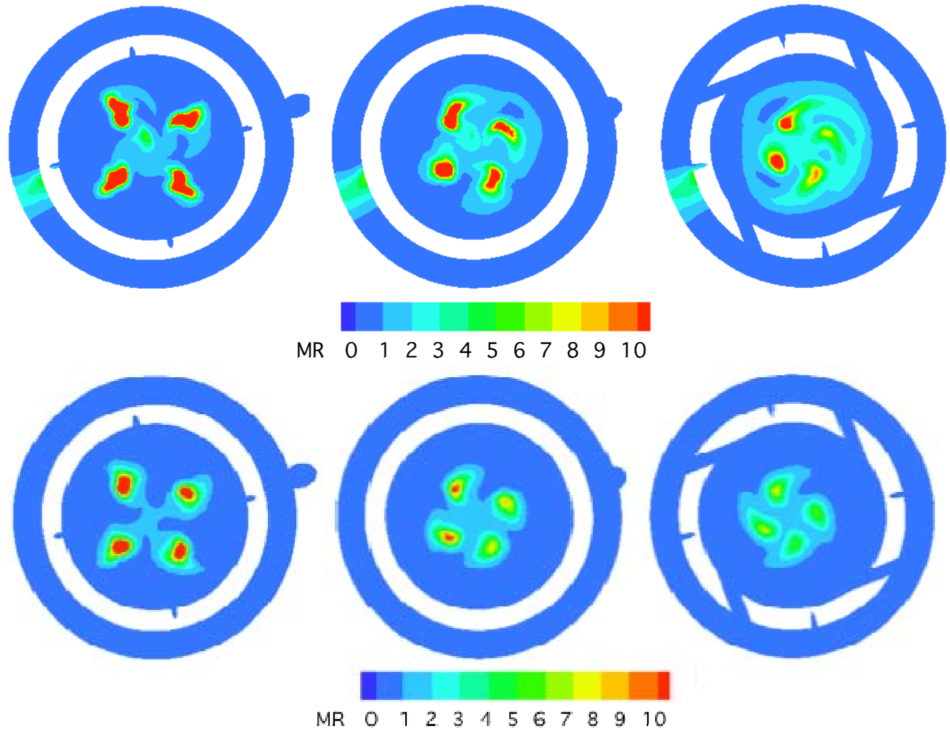

Figure 18.—A comparison of mixture ratio profiles just downstream of the igniter face in the spark region for successful ignition test 1603 (top) and test 1604 with no ignition.

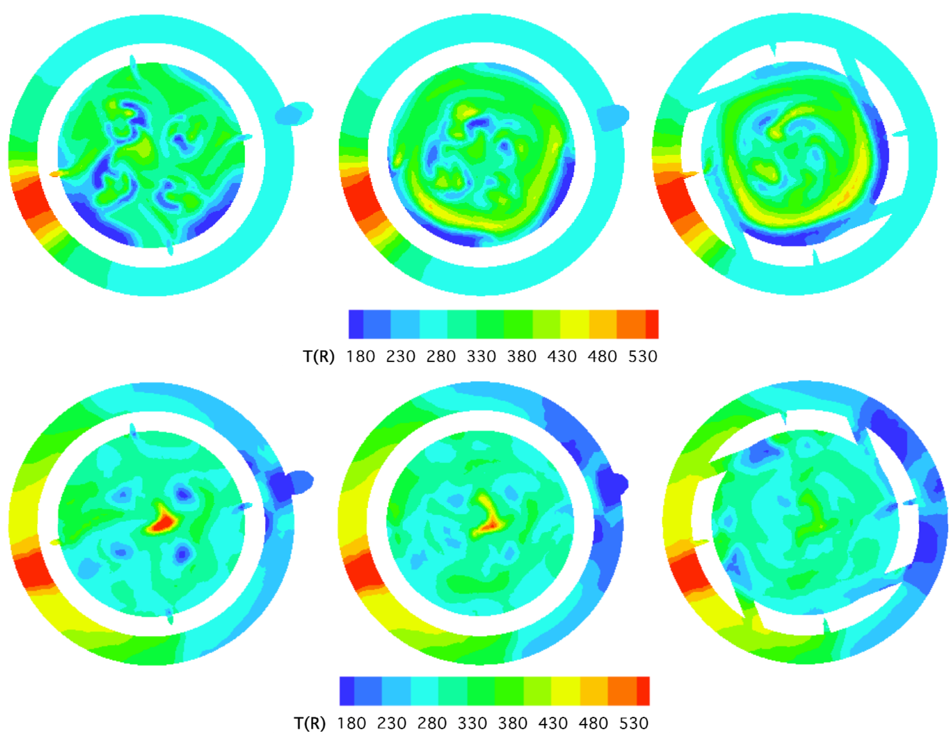

Figure 19.—A comparison of temperature profiles just downstream of the igniter face in the spark region for successful ignition test 1603 (top) and test 1604 with no ignition.

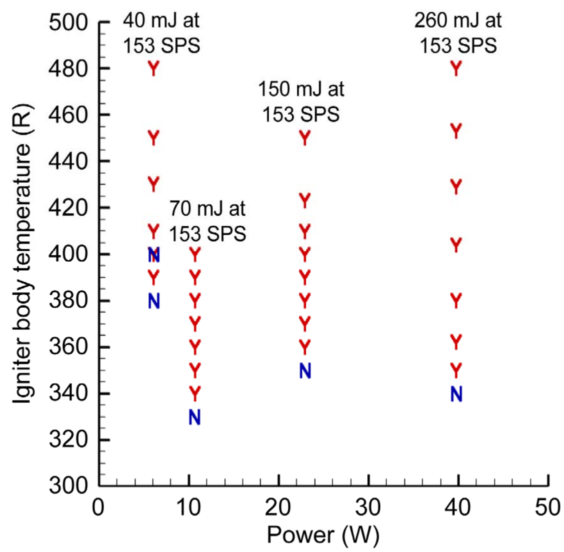

Figure 20.—Cold body ignition boundary versus sparkplug power.

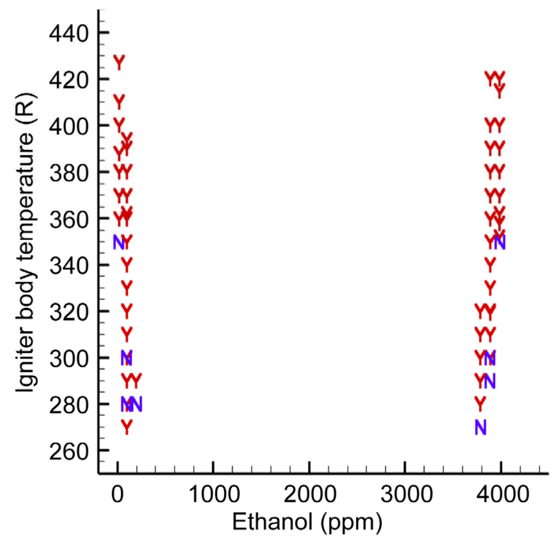

Figure 21.—Cold body ignition boundary for various spark energies.

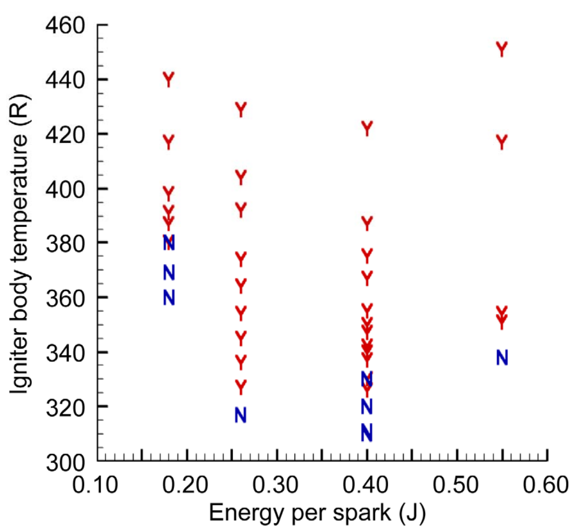

Figure 22.—The effect of sparkplug recess on ignition boundaries.

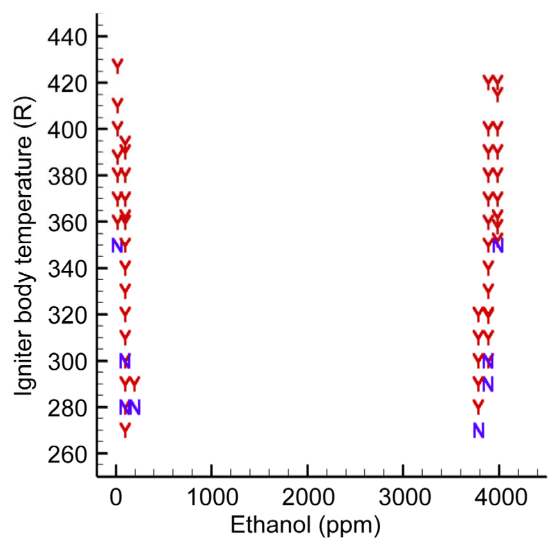

Figure 23.—The effect of methane purity on ignition boundaries.

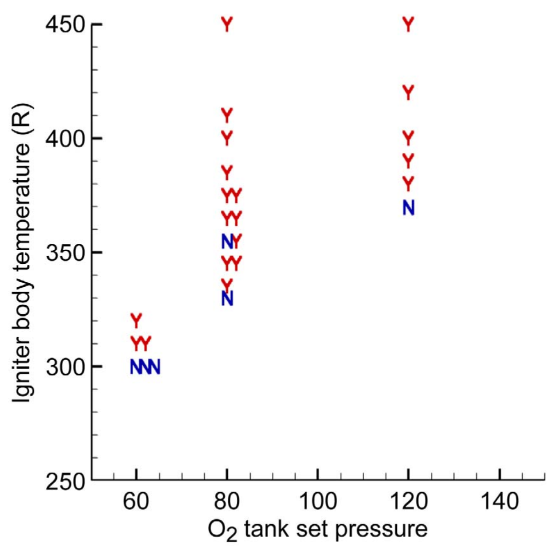

Figure 24.—Cold igniter boundary with chamber/nozzle attached to igniter.

REPORT DOCUMENTATION PAGE						*Form Approved* *OMB No. 0704-0188*
The public reporting burden for this collection of information is estimated to average 1 hour per response, including the time for reviewing instructions, searching existing data sources, gathering and maintaining the data needed, and completing and reviewing the collection of information. Send comments regarding this burden estimate or any other aspect of this collection of information, including suggestions for reducing this burden, to Department of Defense, Washington Headquarters Services, Directorate for Information Operations and Reports (0704-0188), 1215 Jefferson Davis Highway, Suite 1204, Arlington, VA 22202-4302. Respondents should be aware that notwithstanding any other provision of law, no person shall be subject to any penalty for failing to comply with a collection of information if it does not display a currently valid OMB control number. PLEASE DO NOT RETURN YOUR FORM TO THE ABOVE ADDRESS.						
1. REPORT DATE *(DD-MM-YYYY)* 01-11-2008		**2. REPORT TYPE** Technical Memorandum				**3. DATES COVERED** *(From - To)*
4. TITLE AND SUBTITLE LOX/Methane Main Engine Igniter Tests and Modeling						**5a. CONTRACT NUMBER**
						5b. GRANT NUMBER
						5c. PROGRAM ELEMENT NUMBER
6. AUTHOR(S) Breisacher, Kevin, J.; Ajmani, Kumud						**5d. PROJECT NUMBER**
						5e. TASK NUMBER
						5f. WORK UNIT NUMBER WBS 253225.04.01.03.03.03.02
7. PERFORMING ORGANIZATION NAME(S) AND ADDRESS(ES) National Aeronautics and Space Administration John H. Glenn Research Center at Lewis Field Cleveland, Ohio 44135-3191						**8. PERFORMING ORGANIZATION REPORT NUMBER** E-16585
9. SPONSORING/MONITORING AGENCY NAME(S) AND ADDRESS(ES) National Aeronautics and Space Administration Washington, DC 20546-0001						**10. SPONSORING/MONITORS ACRONYM(S)** NASA; AIAA
						11. SPONSORING/MONITORING REPORT NUMBER NASA/TM-2008-215421; AIAA-2008-4757
12. DISTRIBUTION/AVAILABILITY STATEMENT Unclassified-Unlimited Subject Category: 20 Available electronically at http://gltrs.grc.nasa.gov This publication is available from the NASA Center for AeroSpace Information, 301-621-0390						
13. SUPPLEMENTARY NOTES						
14. ABSTRACT The LOX/methane propellant combination is being considered for the Lunar Surface Access Module ascent main engine propulsion system. The proposed switch from the hypergolic propellants used in the Apollo lunar ascent engine to LOX/methane propellants requires the development of igniters capable of highly reliable performance in a lunar surface environment. An ignition test program was conducted that used an in-house designed LOX/methane spark torch igniter. The testing occurred in Cell 21 of the Research Combustion Laboratory to utilize its altitude capability to simulate a space vacuum environment. Approximately 750 ignition test were performed to evaluate the effects of methane purity, igniter body temperature, spark energy level and frequency, mixture ratio, flowrate, and igniter geometry on the ability to obtain successful ignitions. Ignitions were obtained down to an igniter body temperature of approximately 260 R with a 10 torr backpressure. The data obtained is also being used to anchor a CFD based igniter model.						
15. SUBJECT TERMS Combustion; Ignition; Igniter; Methane; Modeling						
16. SECURITY CLASSIFICATION OF:			**17. LIMITATION OF ABSTRACT**	**18. NUMBER OF PAGES**		**19a. NAME OF RESPONSIBLE PERSON** STI Help Desk (email:help@sti.nasa.gov)
a. REPORT U	**b. ABSTRACT** U	**c. THIS PAGE** U	UU	27		**19b. TELEPHONE NUMBER** *(include area code)* 301-621-0390

Standard Form 298 (Rev. 8-98)
Prescribed by ANSI Std. Z39-18